Nuclear Factor I/B is an Oncogene in Small Cell Lung Cancer

Alison L. Dooley[1], Monte M. Winslow[1], Derek Y. Chiang[2,3,4], Shantanu Banerji[2,3], Nicolas Stransky[2], Talya L. Dayton[1], Eric L. Snyder[1], Stephanie Senna[1], Charles A. Whittaker[1], Roderick T. Bronson[5], Denise Crowley[1], Jordi Barretina[2,3], Levi Garraway[2,3], Matthew Meyerson[2,3], Tyler Jacks[1,6]

[1]David H. Koch Institute for Integrative Cancer Research and Department of Biology, Massachusetts Institute of Technology, Cambridge, Massachusetts, USA
[2]The Broad Institute, Cancer Program, Cambridge, Massachusetts, USA
[3]Dana-Farber Cancer Institute, Department of Medical Oncology and Center for Cancer Genome Discovery, Boston, Massachusetts, USA
[4]Current address: Lineberger Comprehensive Cancer Center, 450 West Drive, CB #7295, Chapel Hill, North Carolina, USA
[5]Department of Pathology, Tufts University School of Medicine and Veterinary Medicine, North Grafton, Massachusetts, USA
[6]Howard Hughes Medical Institute, Massachusetts Institute of Technology, Cambridge, Massachusetts, USA

Key Words: Small Cell Lung Cancer, Mouse model, Nuclear Factor I/B

Abstract

Small cell lung cancer (SCLC) is an aggressive cancer often diagnosed after it has metastasized. Despite the need to better understand this disease, SCLC remains poorly characterized at the molecular and genomic levels. Using a genetically-engineered mouse model of SCLC driven by conditional deletion of *Trp53* and *Rb1* in the lung, we identified several frequent, high-magnitude focal DNA copy number alterations in SCLC. We uncovered amplification of a novel, oncogenic transcription factor, Nuclear Factor I/B (*Nfib*) in the mouse SCLC model and in human SCLC. Functional studies indicate that *NFIB* regulates cell viability and proliferation during transformation.

Introduction

Small cell lung cancer (SCLC) is a highly lethal form of cancer that comprises approximately 20% of all lung cancer cases (Wistuba et al. 2001; Meuwissen and Berns 2005). Unfortunately, SCLC is frequently diagnosed only after metastatic spread of the disease, and presently only 5% of patients survive beyond five years after diagnosis (Worden and Kalemkerian 2000; Cooper and Spiro 2006). Some insight has been gained as to the underlying mechanisms of this aggressive disease, including the identification of loss-of-function mutations in the tumor suppressor genes *Trp53* (Yokota et al. 1987; Takahashi et al. 1989; Takahashi et al. 1991) and *RB1* (Harbour et al. 1988; Yokota et al. 1988), which are observed in 75% and 90% of SCLC cases, respectively (Wistuba et al. 2001; Meuwissen and Berns 2005). In addition, MYC family members (C-MYC, L-MYC, and N-MYC) are frequently amplified in SCLC (Nau et al. 1985;

Meuwissen and Berns 2005). However, very little is known about other functionally relevant alterations in SCLC, and a more complete understanding of the disease is required to allow the development of new targeted treatments.

Whole-genome profiling has been utilized to gain information about copy number alterations, point mutations, and translocations in tumors (Campbell et al. 2008; Ley et al. 2008; Mardis et al. 2009). One recent examination of thirty-three primary SCLC tumors and thirteen SCLC cell lines identified MYC family amplifications in 82% of tumors and 62% of cell lines (Voortman et al. 2010). Another study identified 22,000 point mutations in a SCLC cell line, the majority of which were G-T transversions, a hallmark of carcinogens present in tobacco smoke (Toyooka et al. 2003; Lewis and Parry 2004; Pleasance et al. 2010). In other cancer types, comparative studies utilizing mouse models have aided in narrowing lists of candidate genes (Kim et al. 2006; Zender et al. 2006; Zender et al. 2008). Thus, we analyzed the genomic alterations that occur during tumor progression in a mouse model of SCLC to identify oncogenes in this cancer type.

Results and Discussion

Genetically-engineered mouse model of metastatic SCLC

Berns and colleagues have developed a mouse model of SCLC (mSCLC) that involves the inactivation of the *Trp53* and *Rb1* tumor suppressor genes using conditional ("floxed") alleles in $p53^{fl/fl};Rb^{fl/fl}$ mice (Jonkers et al. 2001; Vooijs et al. 2002; Meuwissen et al. 2003; Sage et al. 2003) (Supplemental Fig. S1). Inhalation of

adenovirus containing Cre recombinase results in infection of lung epithelial cells that develop into tumors resembling human SCLC histopathologically (Meuwissen et al. 2003; DuPage et al. 2009) (Supplemental Fig. S1). These mice have a median survival time of 350 days, during which the tumors become malignant and metastatic (Meuwissen et al. 2003) (Supplemental Fig. S1). Similarly to human SCLC, the mSCLC metastasized to the thoracic lymph nodes, liver, adrenal glands, and bone (Meuwissen et al. 2003) (Supplemental Fig. S1). Thus, this model provided a platform with which to identify genetic alterations that occur during tumor progression.

Identification of Nuclear Factor I/B Amplifications

To determine the genetic alterations that occur in mSCLC, primary tumors and metastases were dissected and used for histology, DNA and RNA isolation, as well as for the derivation of cell lines (Supplemental Fig. S1). Each tumor was verified histopathologically to be SCLC and tumor purity was assessed by PCR for the recombined *Trp53* and *Rb1* alleles (Supplemental Fig. S1 and data not shown). The analysis of DNA copy number alterations in murine tumor models has previously aided in the identification of functionally important genes in several human cancers (Kim et al. 2006; Zender et al. 2006; Zender et al. 2008). Thus, we analyzed mSCLC tumors and metastases using next generation sequencing-based DNA copy number analysis (Chiang et al. 2009). These data show that while the majority of the genome was surprisingly unaltered, several high-level focal amplifications and deletions were observed in tumor specimens (Fig. 1A, Supplemental Fig. S2-S4, Supplemental Table

1). In particular, we identified two recurrent focal amplifications centered around 82 Mb and 122 Mb on mouse chromosome 4 and a heterozygous deletion spanning from approximately 148.5 Mb to the end of chromosome 4 (Fig. 1B). Although one of the focal amplifications on chromosome 4 contained a known proto-oncogene involved in SCLC, L-myc (*Mycl1)* (Nau et al. 1985), the other focal amplification contained no genes previously implicated in this disease (Fig. 1C, Supplemental Fig. S3). To identify the relevant targets within the amplified region, the amplification breakpoints were mapped using statistical changepoint analysis of the normalized copy number ratios (Chiang et al. 2009). Nuclear Factor I/B (*Nfib*) was the only gene within this region amplified in each of the samples (Fig. 1C). Further, *Nfib* is located at the apex of the amplified peak in tumors and tumor-derived cell lines (Supplemental Fig. S2). Thus, *Nfib* represents a newly identified amplified gene in SCLC.

Nuclear Factor I/B (*Nfib*) is a CCAAT-box-binding transcription factor that regulates the expression of lung differentiation genes (Santoro et al. 1988; Steele-Perkins et al. 2005). *Nfib* knockout mice have lung hypoproliferation and differentiation defects, in addition to brain defects, and die shortly after birth (Gründer et al. 2002). The chromosomal region containing *Nfib* has been reported to be frequently amplified in a mouse model of prostate cancer (Zhou et al. 2006) and in patients with triple negative breast cancer (Han et al. 2008). Based on the identification of *Nfib* as an amplified gene in SCLC and its potential importance in other prevalent tumor types, we chose to examine *Nfib* further.

The DNA copy number of *Nfib* and the expression of *Nfib* mRNA was determined using real time PCR in a panel of 28 mSCLC-derived cell lines (Fig. 2A, B). Out of 28 cell lines, sixteen had *Nfib* and six had *L-myc* amplifications (Fig. 2A, Supplemental Fig. S5). Notably, four mSCLC cell lines had amplified both *Nfib* and *L-myc* (Supplemental Fig. S5). mSCLC cell lines with increased *Nfib* copy number also expressed high levels of *Nfib* (Fig. 2B). Interestingly, two cell lines with normal *Nfib* copy number expressed high levels of *Nfib* mRNA suggesting that mechanisms other than genomic alteration may increase Nfib levels in SCLC (Fig. 2B).

To confirm *Nfib* amplification in mouse tumors, we performed fluorescence *in situ* hybridization (FISH). FISH confirmed the amplification of *Nfib* in the lymph node metastasis analyzed in Figure 1 (Fig. 2C, D). Interestingly, in a primary tumor we found that *Nfib* amplification clearly correlated with a region of increased Nfib expression (Fig. 2E, F). In normal lung, Nfib protein was localized appropriately to the nucleus of alveolar type II cells (Steele-Perkins et al. 2005) and was also nuclear in mSCLC. Additionally, Nfib protein was detected in a subset of lung neuroendocrine cells (Supplemental Fig. S6). Consistent with data from human tumor samples (Bhattacharjee et al. 2001), Nfib was not detected in lung adenomas that occasionally arise in this mouse model (Supplemental Fig. S7). Further, we observed that both lymph node and liver metastases very frequently expressed high levels of Nfib (Supplemental Fig. S7). These data confirm the amplification and increased expression of *Nfib* in mSCLC tumors and local and distant metastases.

NFIB amplifications in human SCLC

We next examined whether *NFIB* is amplified and/or expressed in human SCLC. Copy number analysis revealed a broad region of amplification on chromosome 9p23 encompassing 210 genes. GISTIC analysis identified approximately a 200 kb minimal region of amplification containing only one gene, *NFIB* (Beroukhim et al. 2007). In total, 16 of 46 human SCLC cell lines had *NFIB* copy number gains (Fig. 3A). Interestingly, 11 of the cell lines with *NFIB* amplification also had *L-MYC* amplification, and 15 out of the 16 cell lines with amplification of *NFIB* displayed additional amplification of one of the *MYC* family members (Supplemental Fig. S5 and data not shown). Increased *NFIB* copy number was confirmed by real time PCR (Supplemental Fig. S8). Additionally, *NFIB* amplification was detected by FISH in 15% of primary human tumor samples (Fig. 3B). We next addressed whether NFIB protein was expressed in human SCLC tumor samples by performing IHC on a tissue microarray containing 68 distinct human SCLC samples. High level NFIB protein expression was noted in 16% of samples and the protein was detectable in 65% of tumors (Fig. 3C and Supplemental Fig. S9). Collectively, these data from both the mouse model and human patients suggest a potentially oncogenic role for *NFIB* in SCLC.

NFIB controls apoptosis and viability in human SCLC

To determine which cellular processes are regulated by NFIB, we used RNA interference (RNAi) to inhibit NFIB in several human SCLC cell lines. In one adherent cell line (NCI-H446), which has high-level *NFIB* amplification and expresses very high

levels of *NFIB*, RNAi-mediated NFIB knockdown caused a dramatic increase in apoptosis and a corresponding decrease in proliferation (Fig. 4A, B and Supplemental Fig. S10). In a second SCLC cell line (NCI-H196), which lacked *NFIB* amplification, NFIB knockdown led to different outcomes depending on the shRNA used, with one inducing apoptosis and the other cellular senescence (Fig. 4C-E and Supplemental Fig. S10). In one final human SCLC cell line (NCI-H82), NFIB knockdown reduced proliferation (Supplemental Fig. S10). Collectively, these data suggest that *NFIB* expression is integral to human SCLC cell line viability and/or continued proliferation likely depending on the NFIB levels or the cellular context of each individual tumor.

Nfib is an oncogene in mSCLC

We next examined whether *Nfib* plays an oncogenic role in the cellular transformation of murine small cell lung tumors. For initial functional studies, we utilized mSCLC cell lines that expressed low levels of endogenous Nfib, in which we then stably expressed Nfib (Supplemental Fig. S11). Ectopic expression of Nfib in two independent mSCLC cell lines increased the number and size of anchorage-independent colonies compared to uninfected cells (Fig. 5A and Supplemental Fig. S11). Furthermore, cells over-expressing Nfib proliferated more quickly under standard culture conditions (Fig. 5B and Supplemental Fig. S11). To assess which pathways were altered by the over-expression of Nfib, we performed gene expression arrays and a Gene Set Enrichment Analysis (GSEA). Within curated gene sets, a number of cancer-related gene sets

correlated with over-expression of Nfib (Supplemental Fig. S12). These data support our hypothesis that Nuclear Factor I/B has oncogenic properties.

We also investigated whether Nfib has oncogenic activity in a heterologous setting by testing whether Nfib could transform wild-type or $p53^{-/-}$ mouse embryonic fibroblasts (MEFs) (Fig. 5C-E and Supplemental Fig. S13). Expressing Nfib significantly increased colony formation in a low-density colony formation assay (Fig. 5C, D, and Supplemental Fig. S13). Additionally, while neither control nor Nfib expressing wild-type MEFs could grow under anchorage-independent conditions, expression of Nfib in $p53^{-/-}$ MEFs dramatically enhanced growth of anchorage-independent colonies (Fig. 5E and Supplemental Fig. S13). Finally, when wild-type MEFs were plated at high density to assay for the ability to overcome contact inhibition of growth, significantly more three-dimensional foci formed when MEFs expressed Nfib (Supplemental Fig. S13).

Interestingly, we observed frequent concurrent amplification and expression of both *Nfib* and *L-myc* (Fig. 1B, Supplemental Fig. S3 and S5). In some cell culture assays, including the formation of three dimensional foci of wild-type MEFs in high density conditions, we observed cooperativity between exogenous L-myc and Nfib, which was significant by the Bliss Independence test (Supplemental Fig. S13). Thus, L-myc and Nfib may act synergistically in some settings.

The use of a genetically-engineered mouse model of SCLC enabled us to interrogate the genomic alterations that occur in SCLC. We identified several high-level focal amplifications and deletions and, notably, uncovered amplification of a novel potential proto-oncogene, Nuclear Factor I/B. This mouse model provides several

advantages over studying this cancer type in humans. First, the tumors are initiated by defined genetic events and the disease progresses in the absence of smoking carcinogen-induced passenger mutations and alterations. Second, a wealth of tumor and metastasis samples can be collected and utilized for DNA, RNA, and protein analyses as well as histology and cell line derivation. And third, tumors can be collected at different stages, with our data indicating that Nfib is highly expressed in the most advanced stages of mSCLC. Interestingly, the human SCLC cell lines in which we demonstrated that NFIB is critical for tumor maintenance were also derived from patient pleural effusions and a lymph node metastasis. Thus, advanced lesions still appear to critically depend on NFIB for cell viability. Given our success in analyzing copy number alterations in mSCLC, future efforts to catalogue point mutations in mSCLC, followed by cross-species analyses, would likely prioritize the daunting number of potentially meaningful mutations being identified in human SCLC (Pleasance et al. 2010). Our study highlights the power of rationally designed mouse models to uncover novel cancer-promoting alterations and uncovered an important proto-oncogenic transcription factors in SCLC.

Materials and Methods

Mice. $p53^{fl/fl}$;$Rb^{fl/fl}$ and $p53^{fl/fl}$;$Rb^{fl/fl}$;$Rosa26^{LSL\text{-}Luciferase/LSL\text{-}Luciferase}$ mice have been described (Jonkers et al. 2001; Vooijs et al. 2002; Meuwissen et al. 2003; Sage et al. 2003) ($Rosa26^{LSL\text{-}Luciferase/LSL\text{-}Luciferase}$ mice are unpublished, Erica Jackson, Tyler Jacks). They were infected intranasally or intratracheally with $2.5x10^7$ or 10^8 PFU of adenovirus,

as previously described (DuPage et al. 2009). Mouse research was approved by the Committee for Animal Care, and conducted in compliance with the Animal Welfare Act Regulations and other federal statutes relating to animals and experiments involving animals, and adheres to the principles set forth in the Guide for the Care and Use of Laboratory Animals, National Research Council, 1996 (Institutional animal welfare assurance no. A-3125-01).

Isolation of Tumor DNA and Production of Cell Lines. Primary tumors from the mouse model were snap frozen for DNA isolation and stored at -80°C. In addition, part of each tumor was kept for histology, cell line preparation, and snap frozen in RNALater (Ambion). To isolate DNA, tumors were digested in 800 μg/mL Proteinase K overnight at 55°C and phenol/chloroform extracted. To dissociate tumors for cell lines, minced tumors were digested in HBSS (without calcium and magnesium), 1 mg/mL Collagenase IV (Worthington Biochemicals), and 0.025% trypsin-EDTA (Gibco) at 37°C for 30 minutes. Following dissociation, samples were quenched in PBS with 10% FBS, incubated in 25 μg/mL DNase I (Sigma), centrifuged, filtered, and plated in standard tissue culture media (DME, 10% FBS, 1% L-glutamine and 50 units/mL Penicillin, 50 μg/mL Streptomycin).

Illumina sequencing and data analysis. Libraries for DNA copy number analysis were prepared from 5 μg of DNA using the Illumina Genomic DNA Sample Preparation Kit. Single-end 35 nucleotide reads were generated using the Illumina Genome Analyzer IIx.

Reads were aligned to the mm9 reference genome with MAQ and filtered for mapping quality greater than 30 (Supplemental Table 2). For each 100 kb genomic window, the number of reads aligning to that window were normalized by the total number of aligned reads in the sample. Copy number ratios were calculated as the number of normalized reads from the tumor sample, divided by the number of normalized reads from the reference 129/SVJ strain. Chromosomal boundaries of copy number changes were identified by changepoint analysis (Chiang et al. 2009). DNA copy number was visualized using the Broad Institute's Integrated Genome Viewer (http://www.broadinstitute.org/igv).

Human SCLC cell line copy number profiling. Affymetrix SNP 6.0 data was obtained from the Cancer Cell Line Encyclopedia (www.broadinstitute.org/ccle). DNA isolation and hybridization arrays were performed as recommended by Affymetrix. Probe normalization, segmentation, and copy-number profiles were determined as previously described (C.G.A.R.N. 2008). Significantly recurrent regions of somatic copy number alterations were identified using the latest GISTIC methodology as described (Beroukhim et al. 2007; Beroukhim et al. 2010).

Immunohistochemistry. Anti-Nfib antibody (Abcam, 1: 500) was used for IHC using standard methods.

References

Beroukhim R, Getz G, Nghiemphu L, Barretina J, Hsueh T, Linhart D, Vivanco I, Lee JC, Huang JH, Alexander S et al. 2007. Assessing the significance of chromosomal aberrations in cancer: methodology and application to glioma. Proc Natl Acad Sci 104: 20007-20012.

Beroukhim R, Mermel CH, Porter D, Wei G, Raychaudhuri S, Donovan J, Barretina J, Boehm JS, Dobson J, Urashima M et al. 2010. The landscape of somatic copy-number alteration across human cancers. Nature 463: 899-905.

Bhattacharjee A, Richards WG, Staunton J, Li C, Monti S, Vasa P, Ladd C, Beheshti J, Bueno R, Gillette M et al. 2001. Classification of human lung carcinomas by mRNA expression profiling reveals distinct adenocarcinoma subclasses. PNAS 98: 13790-13795.

C.G.A.R.N. 2008. Comprehensive genomic characterization defines human glioblastoma genes and core pathways. Nature 455: 1061-1068.

Campbell PJ, Stephens PJ, Pleasance ED, O'Meara S, Li H, Santarius T, Stebbings LA, Leroy C, Edkins S, Hardy C et al. 2008. Identification of somatically acquired rearrangements in cancer using genome-wide massively parallel paired-end sequencing. Nat Genet 40: 722.

Chiang DY, Getz G, Jaffe DB, O'Kelly MJT, Zhao X, Carter SL, Russ C, Nusbaum C, Meyerson M, and Lander ES. 2009. High-resolution mapping of copy-number alterations with massively parallel sequencing. Nat Meth 6: 99-103.

Cooper S and Spiro SG. 2006. Small cell lung cancer: Treatment review. Respirology 11: 241-248.

DuPage M, Dooley AL, and Jacks T. 2009. Conditional mouse lung cancer models using adenoviral or lentiviral delivery of Cre recombinase. Nat Protocols 4: 1064-1072.

Gründer A, Ebel TT, Mallo M, Schwarzkopf G, Shimizu T, Sippel AE, and Schrewe H. 2002. Nuclear factor I-B (*Nfib*) deficient mice have severe lung hypoplasia. Mechanisms of Development 112: 69-77.

Han W, Jung E-M, Cho J, Lee JW, Hwang K-T, Yang S-J, Kang JJ, Bae J-Y, Jeon YK, Park I-A et al. 2008. DNA copy number alterations and expression of relevant genes in triple-negative breast cancer. Genes, Chromosomes and Cancer 47: 490-499.

Harbour JW, Lai SL, Whang-Peng J, Gazdar AF, Minna JD, and Kaye FJ. 1988. Abnormalities in structure and expression of the human retinoblastoma gene in SCLC. Science 241: 353-357.

Jonkers J, Meuwissen R, van der Gulden H, Peterse H, van der Valk M, and Berns A. 2001. Synergistic tumor suppressor activity of BRCA2 and p53 in a conditional mouse model for breast cancer. Nat Genet 29: 418-425.

Kim M, Gans JD, Nogueira C, Wang A, Paik J-H, Feng B, Brennan C, Hahn WC, Cordon-Cardo C, Wagner SN et al. 2006. Comparative Oncogenomics Identifies NEDD9 as a Melanoma Metastasis Gene. Cell 125: 1269-1281.

Lewis PD and Parry JM. 2004. In silico p53 mutation hotspots in lung cancer. Carcinogenesis 25: 1099-1107.

Ley TJ, Mardis ER, Ding L, Fulton B, McLellan MD, Chen K, Dooling D, Dunford-Shore BH, McGrath S, Hickenbotham M et al. 2008. DNA sequencing of a cytogenetically normal acute myeloid leukaemia genome. Nature 456: 66-72.

Mardis ER, Ding L, Dooling DJ, Larson DE, McLellan MD, Chen K, Koboldt DC, Fulton RS, Delehaunty KD, McGrath SD et al. 2009. Recurring mutations found by sequencing an acute myeloid leukemia genome. N Engl J Med 361: 1058-1066.

Meuwissen R and Berns A. 2005. Mouse models for human lung cancer. Genes Dev 19: 643-664.

Meuwissen R, Linn SC, Linnoila RI, Zevenhoven J, Mooi WJ, and Berns A. 2003. Induction of small cell lung cancer by somatic inactivation of both Trp53 and Rb1 in a conditional mouse model. Cancer Cell 4: 181-189.

Nau MM, Brooks BJ, Battey J, Sausville E, Gazdar AF, Kirsch IR, McBride OW, Bertness V, Hollis GF, and Minna JD. 1985. L-myc, a new myc-related gene amplified and expressed in human small cell lung cancer. Nature 318: 69-73.

Pleasance ED, Stephens PJ, O'Meara S, McBride DJ, Meynert A, Jones D, Lin M-L, Beare D, Lau KW, Greenman C et al. 2010. A small-cell lung cancer genome with complex signatures of tobacco exposure. Nature 463: 184-190.

Sage J, Miller AL, Perez-Mancera PA, Wysocki JM, and Jacks T. 2003. Acute mutation of retinoblastoma gene function is sufficient for cell cycle re-entry. Nature 424: 223-228.

Santoro C, Mermod N, Andrews PC, and Tjian R. 1988. A family of human CCAAT-box-binding proteins active in transcription and DNA replication: cloning and expression of multiple cDNAs. Nature 334: 218-224.

Schaffer BE, Park K-S, Yiu G, Conklin JF, Lin C, Burkhart DL, Karnezis AN, Sweet-Cordero EA, and Sage J. 2010. Loss of p130 Accelerates Tumor Development in a Mouse Model for Human Small-Cell Lung Carcinoma. Cancer Research 70: 3877-3883.

Steele-Perkins G, Plachez C, Butz KG, Yang G, Bachurski CJ, Kinsman SL, Litwack ED, Richards LJ, and Gronostajski RM. 2005. The Transcription Factor Gene Nfib Is Essential for both Lung Maturation and Brain Development. Mol Cell Biol 25: 685-698.

Takahashi T, Nau MM, Chiba I, Birrer MJ, Rosenberg RK, Vinocour M, Levitt M, Pass H, Gazdar AF, and Minna JD. 1989. p53: a frequent target for genetic abnormalities in lung cancer. Science 246: 491-494.

Takahashi T, Takahashi T, Suzuki H, Hida T, Sekido Y, Ariyoshi Y, and Ueda R. 1991. The p53 gene is very frequently mutated in small-cell lung cancer with a distinct nucleotide substitution pattern. Oncogene 6: 1775-1778.

Toyooka S, Tsuda T, and Gazdar AF. 2003. The TP53 gene, tobacco exposure, and lung cancer. Human Mutation 21: 229-239.

Vooijs M, te Riele H, van der Valk M, and Berns A. 2002. Tumor formation in mice with somatic inactivation of the retinoblastoma gene in interphotoreceptor retinol binding protein-expressing cells. Oncogene 21: 4635-4645.

Voortman J, Lee JH, Killian JK, Suuriniemi M, Wang Y, Lucchi M, Smith WI, Jr., Meltzer P, and Giaccone G. 2010. Array comparative genomic hybridization-based characterization of genetic alterations in pulmonary neuroendocrine tumors. Proc Natl Acad Sci 107: 13040-13045.

Wistuba II, Gazdar AF, and Minna JD. 2001. Molecular genetics of small cell lung carcinoma. Semin Oncol 28: 3-13.

Worden FP and Kalemkerian GP. 2000. Therapeutic advances in small cell lung cancer. Expert Opin Investig Drugs 9: 565-579.

Yokota J, Akiyama T, Fung Y-KT, Benedict WF, Namba Y, Hanaoka M, Wada M, Terasaki T, Shimosato Y, Sugimura T et al. 1988. Altered expression of the retinoblastoma (RB) gene in small-cell carcinoma of the lung. Oncogene 3: 471-475.

Yokota J, Wada M, Shimosato Y, Terada M, and Sugimura T. 1987. Loss of heterozygosity on chromosomes 3, 13, and 17 in small-cell carcinoma and on chromosome 3 in adenocarcinoma of the lung. Proc Natl Acad Sci 84: 9252-9256.

Zender L, Spector MS, Xue W, Flemming P, Cordon-Cardo C, Silke J, Fan S-T, Luk JM, Wigler M, Hannon GJ et al. 2006. Identification and Validation of Oncogenes in Liver Cancer Using an Integrative Oncogenomic Approach. Cell 125: 1253-1267.

Zender L, Xue W, Zuber J, Semighini CP, Krasnitz A, Ma B, Zender P, Kubicka S, Luk JM, Schirmacher P et al. 2008. An oncogenomics-based in vivo RNAi screen identifies tumor suppressors in liver cancer. Cell 135: 852-864.

Zhou Z, Flesken-Nikitin A, Corney DC, Wang W, Goodrich DW, Roy-Burman P, and Nikitin AY. 2006. Synergy of p53 and Rb Deficiency in a Conditional Mouse Model for Metastatic Prostate Cancer. Cancer Research 66: 7889-7898.

Acknowledgments

We would like to acknowledge D. Feldser, E. Meylan, N. Dimitrova, and T. Papagiannakopoulos for advice and C. Kim-Kiselak for critical reading of the manuscript. We thank Jacks Lab members and T. Parisi for reagents. We are indebted to the Koch Institute Core Facilities: D. Cook and A. Leshinsky (Biopolymers), E. Vasile (Microscopy), and G. Paradis (Flow Cytometry). We thank M. Luo (BioMicro Center) for microarray support and M. Leversha at Sloan Kettering Cancer Center Cytogenetics core facility for FISH. This work was supported by the Ludwig Center for Molecular Oncology at MIT, the Howard Hughes Medical Institute, and in part by the Cancer Center Support (core) grant P30-CA14051 from the National Cancer Institute. T.J. is a Howard Hughes Investigator, the David H. Koch Professor of Biology and a Daniel K. Ludwig Scholar. M.M.W was a Merck Fellow of the Damon Runyon Cancer Research Foundation and a Genentech Postdoctoral Fellow. D.Y.C. is supported by an Alfred P. Sloan Foundation Research Fellowship.

Author Information

Contributions

A.L.D., M.M.W. and T.J. designed the experiments. A.L.D., M.M.W., T.D., S.S. performed the experiments. D.Y.C. analyzed the mouse copy number analysis, and C.W. provided bioinformatics support. S.B., N.S., J.B., L.G., and M.M. performed the human copy number analysis. E.S. and R.B. provided histopathological analysis and D.C. provided histological support.

Competing financial interests

The authors declare no competing financial interests.

Corresponding author

Correspondence to: Dr. T. Jacks, Koch Institute and Department of Biology, Massachusetts Institute of Technology, 77 Massachusetts Avenue, E17-517, Cambridge, Massachusetts, USA. E-mail: tjacks@mit.edu

Figure Legends

Figure 1. Nuclear Factor I/B is amplified in murine SCLC tumors. (*A*) Log_2 ratio of tumor to somatic DNA copy number across the whole genome of a mSCLC lymph node metastasis cell line. The X chromosome has a copy number ratio of 2 due to the male reference genome while the sample was derived from a female mouse. (*B*) DNA copy number ratio of chromosome 4 of the same sample as in (*A*). Interestingly, the region between the two focal amplifications is near diploid and contains the tumor suppressor gene, *Cdkn2a*. Despite the well-known role of *Cdkn2a* in regulating p53 and Rb, which are already deleted in tumors, the fact that the copy number of this gene is kept low is consistent with this locus regulating other Rb family members (Schaffer et al. 2010). Copy number data is plotted as the tumor to somatic copy number ratio. (*C*) Integrated genome viewer (IGV) plot of the DNA copy number of position 79.5 to 84.5 Mb on chromosome 4. Scale bar indicates the log_2 copy number ratio of tumor to somatic

reference sample. Dotted line indicates the boundaries of the minimally conserved region. T: primary lung tumor, Liv: liver metastasis, LN: lymph node metastasis, gray labels: tumor samples, black labels: cell lines.

Figure 2. Nuclear Factor I/B is expressed in mSCLC. (*A*) *Nfib* is amplified in tumor- and metastasis-derived cell lines. A DNA copy number ratio greater than 1.2 was considered to be amplified, as determined by real time PCR on genomic DNA. (*B*) Cell lines with increased copy number of the *Nfib* locus also have increased expression of *Nfib.* (*C*) FISH analysis on a lymph node metastasis confirming known amplification of *Nfib* from copy number analysis. Inset is of a cell with amplified *Nfib*. (*D*) Matching Nfib IHC on the same lymph node metastasis as in (*C*), which has high Nfib expression. (*E*) FISH analysis of a lung tumor illustrating amplification of *Nfib* in a subset of tumor cells. Left inset illustrates a cell with normal *Nfib* copy number, right inset is a cell with amplified *Nfib*. (*F*) Matching Nfib IHC on the same lung tumor as in (*E*) demonstrating increased Nfib expression in the region with *Nfib* amplification. (*C-F*: scale bar is 20 μm, *C, E*: red: Nfib probe, green: control chromosome 4qA1 probe, blue: DAPI.)

Figure 3. Nuclear Factor I/B is amplified and expressed in human small cell lung cancer. (*A*) IGV plot of 46 human SCLC cell lines from position 11.1 -17.2 Mb on human chromosome 9. Dotted line indicates the boundaries of the minimally conserved region. Scale bar indicates the $\log_2$ copy number ratio of tumor to somatic reference sample. (*B*) *NFIB* was amplified in human tissue samples, as detected by *NFIB* FISH. Top panel is a

representative sample with normal *NFIB* copy number. Bottom panel is a representative sample with amplified *NFIB*. Red: NFIB probe, green: control chromosome 9 9q12 probe, blue: DAPI. Scale bar is 10 μm. (*C*) Quantification of NFIB expression in human SCLC tissue samples as detected by IHC for NFIB.

Figure 4. NFIB knockdown induces death and reduces proliferation in human SCLC. (*A*) NFIB knockdown increases the percentage of cleaved caspase 3 (CC3) positive cells in the adherent cell line, NCI-H446, by FACS compared to control (Cont.) infected cells. (*B*) Quantification of BrdU incorporation by FACS following NFIB knockdown in the same cell line as (*A*). (*C*) NFIB shRNA1 induces apoptosis, as observed in an increase in the percentage of CC3 positive cells in the adherent cell line, NCI-H196, by FACS. (*D*) Reduced BrdU incorporation as detected by FACS following NFIB knockdown in the same cell line as (*C*). (*E*) Representative pictures of senescence-associated ß-galactosidase staining (SA-ßgal) in an adherent cell line, NCI-H196, following control (left) or NFIB (right) knockdown with shRNA2. Quantification of the SA-ßgal staining is shown in the right panel. (** p value < 0.005, *** p value < 0.0005, compared to cont.).

Figure 5. Nfib is a novel oncogene in murine SCLC. (*A*) Quantification of the number of soft agar colonies in the uninfected or stably expressing Nfib cell line. The values represent the mean +/- standard deviation of triplicate plates. (*B*) Growth curve of a primary tumor cell line, 3151T4, either uninfected or stably expressing Nfib. (*C*) Wild type MEFs either uninfected or infected with Nfib expressing viruses were plated at a

low density and assayed for colony formation. Colonies were visualized using crystal violet and quantified. Values represent the mean +/- standard error of the mean (SEM) of the total number of colonies in triplicate plates of both experiments utilizing two different MEF preparations. (*D*) $p53^{-/-}$ MEFs either uninfected or infected with Nfib expressing viruses were plated at a low density and assayed for colony formation. Colonies were visualized using crystal violet and quantified. Values represent the mean +/- SEM of the total number of colonies in triplicate plates of both experiments utilizing two different MEF preparations. (*E*) $p53^{-/-}$ MEFs either uninfected or infected with Nfib expressing viruses were plated in soft agar and assayed for anchorage-independent colony formation. Colonies were visualized using crystal violet and quantified. Values represent the mean +/- SEM of the number of colonies in nine camera views of triplicate plates in experiments utilizing two different MEF preparations. (**: p value < 0.005, ***: p value < 0.0005).

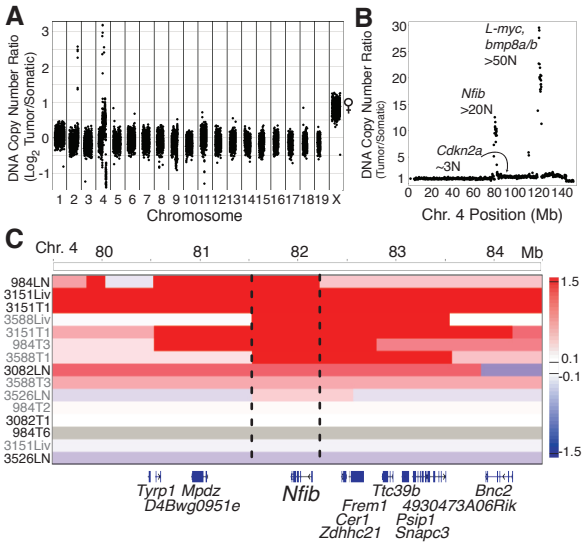
A
DNA Copy Number Ratio
(Log2 Tumor/Somatic)
3
2
1
0
-1
1 2 3 4 5 6 7 8 9 10 11 12 13 14 15 16 17 18 19 X
Chromosome
B
DNA Copy Number Ratio
(Tumor/Somatic)
30
25
20
15
10
5
1
L-myc,
bmp8a/b
>50N
Nfib
>20N
Cdkn2a
~3N
0 20 40 60 80 100 120 140
Chr. 4 Position (Mb)
C
Chr. 4
80
81
82
83
84
Mb
984LN
3151Liv
3151T1
3588Liv
3151T1
984T3
3588T1
3082LN
3588T3
3526LN
984T2
3082T1
984T6
3151Liv
3526LN
1.5
0.1
-0.1
-1.5
Tyrp1
Mpdz
D4Bwg0951e
Nfib
Ttc39b
Frem1
Cer1
Zdhhc21
4930473A06Rik
Psip1
Snapc3
Bnc2

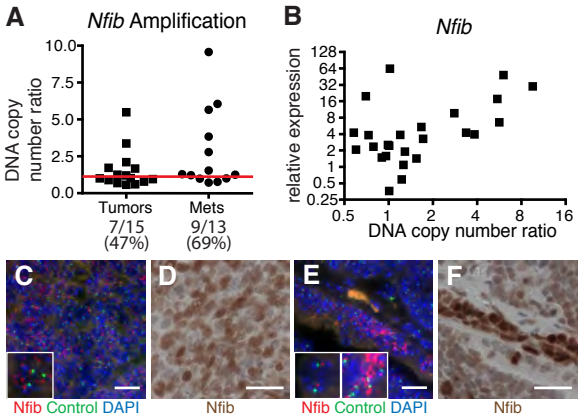
A
Nfib Amplification
DNA copy number ratio
10.0
7.5
5.0
2.5
0.0
Tumors
7/15
(47%)
Mets
9/13
(69%)
B
Nfib
relative expression
128
64
32
16
8
4
2
1
0.5
0.25
0.5
1
2
4
8
16
DNA copy number ratio
C
D
E
F
Nfib Control DAPI
Nfib
Nfib Control DAPI
Nfib

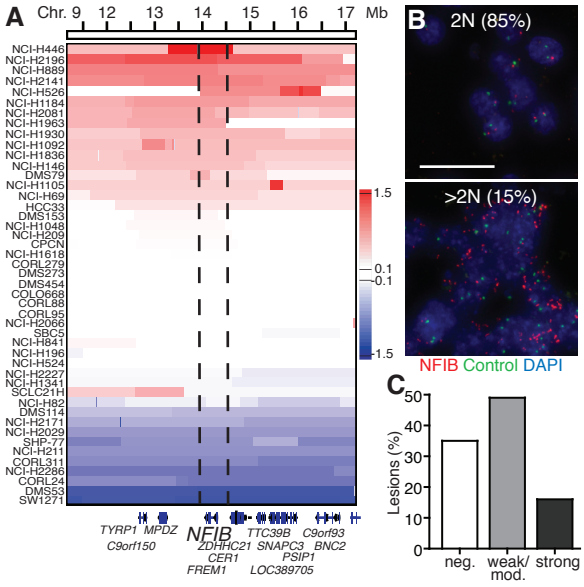
A
Chr. 9 12 13 14 15 16 17 Mb
NCI-H446
NCI-H2196
NCI-H889
NCI-H2141
NCI-H526
NCI-H1184
NCI-H2081
NCI-H1963
NCI-H1930
NCI-H1092
NCI-H1836
NCI-H146
DMS79
NCI-H1105
NCI-H69
HCC33
DMS153
NCI-H1048
NCI-H209
CPCN
NCI-H1618
CORL279
DMS273
DMS454
COLO668
CORL88
CORL95
NCI-H2066
SBC5
NCI-H841
NCI-H196
NCI-H524
NCI-H2227
NCI-H1341
SCLC21H
NCI-H82
DMS114
NCI-H2171
NCI-H2029
SHP-77
NCI-H211
CORL311
NCI-H2286
CORL24
DMS53
SW1271
1.5
0.1
-0.1
-1.5
TYRP1 MPDZ
C9orf150
NFIB
ZDHHC21 CER1
FREM1
TTC39B SNAPC3 PSIP1
LOC389705
C9orf93 BNC2
B
2N (85%)
>2N (15%)
NFIB Control DAPI
C
Lesions (%)
50
40
30
20
10
0
neg.
weak/ mod.
strong

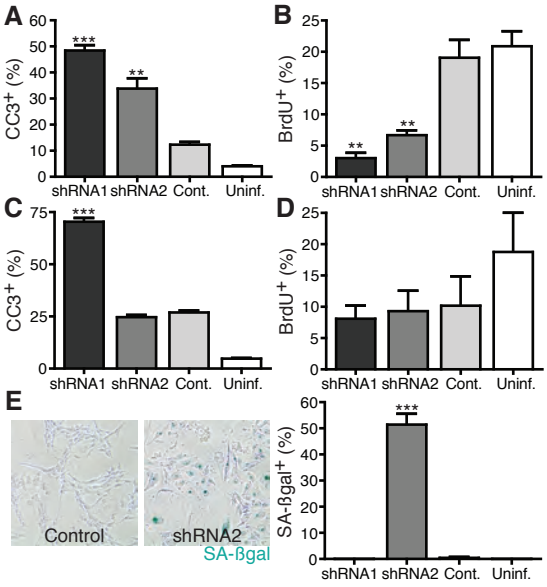
A
CC3+ (%)
60
50
40
30
20
10
0
***
**
shRNA1 shRNA2 Cont. Uninf.
B
BrdU+ (%)
25
20
15
10
5
0
**
**
shRNA1 shRNA2 Cont. Uninf.
C
CC3+ (%)
75
50
25
0
***
shRNA1 shRNA2 Cont. Uninf.
D
BrdU+ (%)
25
20
15
10
5
0
shRNA1 shRNA2 Cont. Uninf.
E
Control
shRNA2
SA-ßgal
SA-ßgal+ (%)
60
50
40
30
20
10
0
***
shRNA1 shRNA2 Cont. Uninf.

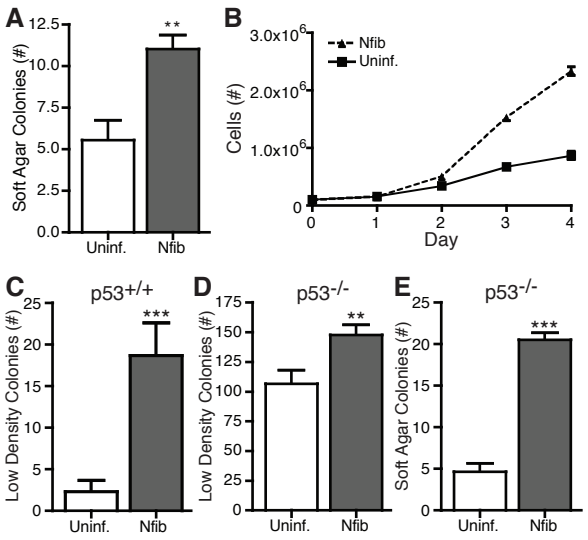
A
Soft Agar Colonies (#)
12.5
10.0
7.5
5.0
2.5
0.0
**
Uninf.
Nfib
B
Cells (#)
3.0x10^6
2.0x10^6
1.0x10^6
0
Nfib
Uninf.
0
1
2
3
4
Day
C
p53+/+
Low Density Colonies (#)
25
20
15
10
5
0
***
Uninf.
Nfib
D
p53-/-
Low Density Colonies (#)
175
150
125
100
75
50
25
0
**
Uninf.
Nfib
E
p53-/-
Soft Agar Colonies (#)
25
20
15
10
5
0
***
Uninf.
Nfib

Nuclear Factor I/B is an Oncogene

in Small Cell Lung Cancer

Alison L. Dooley[1], Monte M. Winslow[1], Derek Y. Chiang[2,3,4], Shantanu Banerji[2,3], Nicolas Stransky[2], Talya L. Dayton[1], Eric L. Snyder[1], Stephanie Senna[1], Charles A. Whittaker[1], Roderick T. Bronson[5], Denise Crowley[1], Jordi Barretina[2,3], Levi Garraway[2,3], Matthew Meyerson[2,3], Tyler Jacks[1,6]

[1]David H. Koch Institute for Integrative Cancer Research and Department of Biology, Massachusetts Institute of Technology, Cambridge, Massachusetts, USA
[2]The Broad Institute, Cancer Program, Cambridge, Massachusetts, USA
[3]Dana-Farber Cancer Institute, Department of Medical Oncology and Center for Cancer Genome Discovery, Boston, Massachusetts, USA
[4]Current address: Lineberger Comprehensive Cancer Center, 450 West Drive, CB #7295, Chapel Hill, North Carolina, USA
[5]Department of Pathology, Tufts University School of Medicine and Veterinary Medicine, North Grafton, Massachusetts, USA
[6]Howard Hughes Medical Institute, Massachusetts Institute of Technology, Cambridge, Massachusetts, USA

Supplemental Information

Supplemental Figure Legends

Supplemental Figure 1. Tumor progression and metastasis in a mouse model of small cell lung cancer. (*A*) Schematic of the mouse model. Exon 19 and exons 2-10 are flanked by loxP sites (floxed) in the *Rb1* and *Trp53* genes ($p53^{fl/fl};Rb^{fl/fl}$), respectively. Following Cre recombinase-mediated recombination, the exons are deleted. (*B*) An *in situ* small cell lung lesion 8 months after infection. (*C*) High magnification of an invasive tumor. At later stages, tumors disseminate within the lung to the (*D*) blood vessels and (*E*) lymphatic vessels, and metastasize locally to the (*F*) lymph nodes, and distantly to the (*G*) liver, (*H*) adrenal glands and (*I*) bone. (*J*) Detection of a bone metastasis using

luciferase imaging of a *p53*$^{fl/fl}$;*Rb*$^{fl/fl}$;*Rosa26*$^{LSL\text{-}Luciferase/LSL\text{-}Luciferase}$ mouse. (*K*) Micro-computed tomography imaging of the bone metastasis. The bone metastasis is osteolytic, consistent with metastatic human SCLC. (left panel: right knee with bone metastasis, right panel: normal left knee.) (*L*) Kaplan-Meier survival curve of mice infected with two different titers of adenovirus expressing Cre recombinase. (squares: $2.5x10^7$ PFU, median latency: 475 days; diamonds: $1x10^8$ PFU, median latency: 350 days). (*B-I*): Hematoxylin and eosin stain.

Supplemental Figure 2. Nfib is located at the peak of the amplification in mSCLC. (*A*) Focally amplified peak containing Nuclear Factor I/B is shown in two tumors. (*B*) Focally amplified peak containing Nuclear Factor I/B is shown in two cell lines. Copy number data is plotted as the tumor to somatic copy number ratio. T: primary lung tumor, Liv: liver metastasis, LN: lymph node metastasis, gray labels: tumor samples, black labels: cell lines.

Supplemental Figure 3. Amplification of *L-myc* in murine small cell lung tumors and cell lines. (*A*) Amplification of *L-myc (Mycl1)* in four cell lines analyzed using Illumina sequencing-based DNA copy number analysis. T: primary lung tumor, Liv: liver metastasis, LN: lymph node metastasis. (*B*) Real time PCR on genomic DNA for amplification of the *L-myc* locus indicates that *L-myc* is amplified in tumor- and metastasis-derived cell lines. A DNA copy number ratio greater than 1.2 was considered an amplification, as determined by real time PCR on genomic DNA. (*C*) Real time PCR

indicates that cell lines that express high levels of *Nfib* also express high levels of *L-myc*. (*D*) IGV display of copy number from 120-8-124.8 Mb on chromosome 4. The samples are organized from highest *L-myc* amplification to lowest. Scale bar indicates the $\log_2$ copy number ratio of tumor to somatic reference sample. Dotted line indicates the boundaries of the minimally conserved region. T: primary lung tumor, Liv: liver metastasis, LN: lymph node metastasis, gray labels: tumor samples, black labels: cell lines.

Supplemental Figure 4. mSCLC samples contain focal amplifications and deletions. (*A*) IGV plot of DNA copy number changes in all samples across the genome. Samples are plotted as the $\log_2$ ratio of tumor to somatic copy number. Scale bar indicates the $\log_2$ copy number ratio of tumor to somatic reference sample. The dotted line indicates the boundaries of the minimally conserved region. T: primary lung tumor, Liv: liver metastasis, LN: lymph node metastasis, gray labels: tumor samples, black labels: cell lines.

Supplemental Figure 5. Co-amplification of *L-myc* and *Nfib* in SCLC. (*A*) Number of mSCLC cell lines with amplifications of *Nfib*, *L-myc* or both *Nfib* and *L-myc*. A DNA copy number ratio greater than 1.2 was considered amplified, as determined by real time PCR on genomic DNA. (*B*) Number of human SCLC cell lines with amplifications of *NFIB* and/or *L-MYC*. A DNA copy number ratio greater than 1.2 was considered amplified, as determined by the copy number profiling.

Supplemental Figure 6. Nfib protein is expressed in lung neuroendocrine cells. (*A*) Percent of neuroendocrine bodies that contain Nfib-expressing cells. Lung neuroendocrine cells express Nfib as detected by double IHC for a neuroendocrine marker, calcitonin gene-related peptide (CGRP, red, cytoplasmic) and Nfib (brown, nuclear). (*B*) Representative image of a neuroendocrine body that lacks Nfib-expressing cells ($CGRP^-Nfib^-$). (*C*) Representative image of a neuroendocrine body that contains Nfib-expressing cells ($CGRP^+Nfib^+$). (*B*, *C*: 40X objective)

Supplemental Figure 7. Nfib protein is expressed in mSCLC. (*A*) Nfib can be detected by IHC in an *in situ* SCLC lesion. (*B*) Nfib is expressed in an invasive small cell lung tumor. (*C*) Nfib is expressed in a lymph node metastasis. (*D*) Nfib is expressed in a liver metastasis. T: liver metastasis, Liv: normal liver. (*E*) Nfib is not expressed in adenomas that arise in the mouse model. A: adenoma, L: normal lung. (*A*, *C*: 20X objective, scale bar is 100 μm; *B, D*: 10X objective, scale bar is 200 μm, *E*: 20X objective) (*F*) Percent of lesions positive (dark gray), weak (light gray), and negative (white) for Nfib expression in lung tumors that are *in situ*, invasive (Inv.), disseminated (Dis.) as well as lymph node (LN) and liver metastases.

Supplemental Figure 8. *NFIB* is amplified in human SCLC cell lines. (*A*) *NFIB* amplifications were confirmed by real time PCR on genomic DNA. All cell lines are NCI cell lines, except where otherwise noted.

Supplemental Figure 9. NFIB is expressed in human SCLC samples. (*A*) Representative images of human SCLC samples with negative, weak/moderate, or high NFIB expression as detected by IHC. NFIB protein expression was graded on a scale of 0 (not expressed) to 3 (highly expressed). The scale bar is 200 μm.

Supplemental Figure 10. NFIB knockdown in human SCLC cell lines. (*A*) Two hairpins knocked down NFIB in an adherent cell line, NCI-H446. (*B*) Western blot demonstrating NFIB knockdown in NCI-H196 using the same two hairpins as in (*A*). (*C*) NFIB knockdown is detected by Western blotting in NCI-H82. (*D*) NFIB knockdown reduces proliferation in NCI-H82, as assessed by BrdU incorporation detected by FACS. Values represent the mean +/- standard deviation of duplicate wells of a representative experiment. (Cont.: control GFP shRNA, Uninf.: uninfected cell line)

Supplemental Figure 11. Nfib is an oncogene in mSCLC cell lines. (*A*) Stable expression of Nfib and/or L-myc in a mouse primary SCLC cell line (3151T4) with low endogenous expression of both Nfib and L-myc. (*B*) Crystal violet staining of soft agar colonies in the uninfected cell line or cell line stably expressing Nfib and/or L-myc. Images are representative of two separate experiments and visualized using crystal violet staining. (C) Quantification of the number of soft agar colonies in the uninfected cell line or cell line stably expressing Nfib, L-myc or L-myc & Nfib. The values represent the mean +/- standard deviation of triplicate plates. (*D*) Growth curve of a primary tumor

cell line, 3151T4, either uninfected or stably expressing Nfib, L-myc or L-myc & Nfib. (*E*) Growth curve of a primary tumor cell line, 3583T3, either uninfected or stably expressing Nfib, L-myc or L-myc & Nfib. (*B-E*: Uninfected and Nfib results are also shown in Figure 5B) (*D, E*) The slope decreases from day 3 to 4 because the cells were reaching confluency after three days. Values represent the mean +/- standard error of the mean of two separate experiments, each performed in triplicate. (*: p value < 0.05, **: p value < 0.005).

Supplemental Figure 12. Significant curated gene sets from the Gene Set Enrichment Analysis (GSEA). Curated gene sets of interest following expression of Nfib in mouse SCLC cell lines. A description of each of the gene sets is included. The values in the table represent the normalized enrichment score (NES). A FDR q-value less than 0.05 was required to be significant.

Supplemental Figure 13. Nfib is an oncogene in mouse embryonic fibroblasts. (*A*) Western blot demonstrating stable expression of Nfib and/or L-myc in wild type and $p53^{-/-}$ MEFs. (*B*) Crystal violet staining and quantification of low density colonies in wild type MEFs or wild type MEFs stably expressing Nfib and/or L-myc. Images are representative of two different MEF preparations and visualized using crystal violet staining. Values represent the mean +/- SEM of the total number of colonies in triplicate plates utilizing two different MEF preparations. (*C*) Crystal violet staining and quantification of low density colonies in $p53^{-/-}$ MEFs stably expressing Nfib and/or L-

myc. Images are representative of two different MEF preparations and visualized using crystal violet staining. Values represent the mean +/- SEM of the total number of colonies in triplicate plates utilizing two different MEF preparations. (*D*) MEFs either uninfected or infected with Nfib and/or L-myc expressing viruses were plated at a high density and assayed for three-dimensional colony formation. Colonies were visualized using crystal violet and quantified. Values represent the mean +/- SEM of the total number of foci in triplicate plates utilizing two different MEF preparations. (*E*) Quantification of the number of soft agar colonies in the uninfected MEFs or MEFs stably expressing Nfib, L-myc or L-myc & Nfib. The values represent the mean +/- SEM of triplicate plates. (*: p value < 0.05, **: p value < 0.005, ***: p value < 0.0005).

Supplemental Table 1. Copy number alterations in mSCLC tumor and cell line samples. An amplification has a somatic to reference copy number ratio greater than or equal to 1.3 and a deletion has a copy number ratio of less than or equal to 0.7. In addition, the X chromosome (Chr. 20) appears to be amplified (copy ratio of 2) if the tumor sample was derived from a female mouse because the reference genome is male. We have removed all amplifications occurring on Chr. 20 if this is the case. We have flagged all amplifications that occurred due to strain differences in the somatic and reference genomes (Germline CNV = “Y”).

Supplemental Table 2. Read depth of Illumina sequencing of each mSCLC tumor and cell line sample. Samples correspond to those shown in Figure 1, where T: primary lung

tumor, Liv: liver metastasis, LN: lymph node metastasis, gray labels: tumor samples, black labels: cell lines. Total reads and confidently aligned reads (mapping quality greater than 30) are shown.

Supplemental Methods

Mouse imaging. Bioluminescence imaging was performed according to manufacturer's instructions (Xenogen). Micro-computed tomography (GE Healthcare) was performed on fixed specimens as previously described (Meylan et al. 2009) with a 27 μM voxel size.

Identification of germline amplifications. Germline copy number variants were identified by first identifying regions with similar start and end positions with respect to the mouse reference genome, within statistical sampling error. At an average sampling density of ~4.4 million aligned reads per sample, an average distance between reads of ~600 bp is expected. Thus, a window size of 12 kb (~20 adjacent reads) was used as the expected resolution for the boundaries of copy number variants. We also expected that germline copy number variants would occur in at least 25% of samples (at least 4 samples). A simple filter was applied to identify putative germline copy number variants. We sorted the left coordinates for all predicted copy number segments. Clusters of left boundaries from 4 different tumors within 12 kb were flagged, and adjacent clusters within 100 kb were merged. The same procedure was performed for the right breakpoints. Segments with both left and right breakpoints meeting these criteria were flagged as potential germline copy number variants (denoted in column "B" in Supplementary Table 1). With these filtering criteria, 76 of the 686 predicted copy number segments corresponded to 14 potential germline copy number variants.

RNA purification, reverse transcription, and real time PCR. RNA was isolated following manufacturer's instructions for TRIzol (Invitrogen). 1.5 μg of RNA was reverse transcribed following manufacturer's instructions for High-Capacity cDNA Reverse Transcription (Applied Biosystems). cDNA was then diluted 1:10 for real time PCR reactions. Real time PCR reactions on genomic DNA were performed using 100 ng (mouse cell lines) or 200 ng (human cell lines) of DNA. All real time PCR reactions were performed using SYBR green (Applied Biosystems). Reactions were performed in triplicate and normalized to the levels of an internal control and analyzed using the comparative Ct method.

Genomic DNA primers:

Organism	**Name**	**Sequence**
Mouse	Nfib F	5' ATTGCTTCACCCGGCGTTCTGTTT
Mouse	Nfib R	5' AGGGTGCCAAGACAGGTGTGAAAT
Mouse	L-myc F	5' AGACTCAGGCCTGCTC
Mouse	L-myc R	5' GATTTCAAACAGCGGTAGATAG
Mouse	Chromosome 5 control F	5' GAAGAAATTAGAGGGCATGCTTC
Mouse	Chromosome 5 control R	5' CTTCTCCCAGTGACCTTATGTA
Human	NFIB F	5' TTATTCCTCAGCGCCCATAACCCA
Human	NFIB R	5' GGTGGAGAAGACAGAGACCTCTGA
Human	L-MYC F	5' ACTGCACTCCCAGCCTCGAA
Human	L-MYC R	5' TGAGAAGAGCCAATGCCTGACCT
Human	NUCLEOLIN F	5' AAACTTTTGCGACGCGTACG
Human	NUCLEOLIN R	5' GGGACTCCGACTAGGGCC

cDNA primers:

Organism	**Name**	**Sequence**
Mouse	*Nfib* F	5' GGGACTAAGCCCAAGAGACC
Mouse	*Nfib* R	5' GTCCAGTCACAAATCCTCAGC

Mouse	*L-myc* F	5' ACTCCTAGTCTGGAAGCCAGTAAC
Mouse	*L-myc* R	5' ACGGTCACCACGTCAATCTCTTCA
Mouse	*Gapdh* F	5' AGCTTGTCATCAACGGGAAG
Mouse	*Gapdh* R	5' TTTGATGTTAGTGGGGTCTCG
Human	*NFIB* F	5' GCCACAATGATCCTGCCAAGAA
Human	*NFIB* R	5' GGTGGAGAAGACAGAGACCTCTGA
Human	*L-MYC* F	5' ACTGCACTCCCAGCCTCGAA
Human	*L-MYC* R	5' TGATGGTGACCGGCTTCCGAATAC
Human	*GAPDH* F	5' AGCCACATCGCTCAGACAC
Human	*GAPDH* R	5' GCCCAATACGACCAAATCC

Immunohistochemistry. Slides used for the single Nfib IHC were deparaffinized, boiled in 10mM sodium citrate buffer pH 6 in a pressure cooker, washed in H_20, and incubated in 3% H_20_2 for 10 minutes. Slides were blocked for avidin and biotin (Vector Laboratories), blocked in 10% goat serum, and incubated overnight in 1:500 anti-NFIB antibody (Abcam). Slides were incubated in biotinylated secondary antibody and then in ABC reagent (ABC kit, Vectastain), signal was detected with a DAB peroxidase substrate kit (Vector Laboratories), and counterstained with hematoxylin. Double IHC was performed sequentially using the Autostainer 360 (Thermo Scientific). Antigen retrieval was performed using the Thermo Pre-treatment module. Anti-Nfib staining (Abcam, 1:1000) was performed first and signal was detected using DAB and was followed by anti-CGRP staining (Sigma, 1:5000), which was detected using Fast Red.

Fluorescence In Situ Hybridization. Human tissue arrays (LC2001 and LC2082) were purchased from US Biomax, Inc. Human BAC clones RP11-355C15 and RP11-1107G7 (spanning *NFIB* in 9p22-23), and mouse BAC clones RP23-386C23 and RP23-132D24

(for *Nfib* in 4qC3), together with proximal MMU4 reference clone RP23-458D19 were utilized in FISH analyses (BACPAC resources). BAC DNA was isolated by standard alkaline lysis and labeled with Red dUTP (*NFIB, Nfib*) or Green dUTP (reference probe) (Abbott Molecular, Inc., Des Plaines, IL) by nick translation. Human cosmid clone cCMP9.27, containing chromosome-specific satellite 3 repeats in 9q12, was used as reference on the human TMAs. Mouse reference BAC RP23-59B17 was part of a 1Mb clone set kindly proved by YJ Chung (Chung et al. 2004). The samples were imaged with an Applied Precision deconvolution microscope, using a 60X, NA 1.3 oil objective, and Softworx software. The acquired z-stack images (5 microns thick sample, 0.2 micron/z section) were deconvolved, and a maximum projection was generated for each z-stack (Koch Institute Microscopy Core Facility).

Immunoblotting. Anti-NFIB antibody (Active Motif, 1: 2000), anti-MYCL1 (Santa Cruz, clone C-20, 1:200), anti-Hsp90 (BD Transduction Laboratories, 1:20000) were used for western blotting following standard methods.

Human SCLC cell line functional experiments. Human SCLC cell lines were obtained from ATCC. Individual clones from the TRC-Hs1.0 library were used for NFIB knockdown in human SCLC cell lines (shRNA #1: TRCN0000014680, CCGTGCTGTGTCTTATCCAAT, shRNA #2: TRCN0000014681, GCACGAAAGAGATCAAGATAT, Control (GFP shRNA): GCAAGCTGACCCTGAAGTTCA). All human cell lines were maintained in RPMI

supplemented with 10% FBS, 1% L-glutamine and 50 units/mL Penicillin, 50 μg/mL Streptomycin. Cells were infected with NFIB or control vectors, and after two days were selected using puromycin (Sigma). Cleaved caspase 3 (CC3) staining was performed according to manufacturer's instructions for flow cytometry staining (Cell Signaling). For cell cycle analysis, cells were incubated for 1 hour with BrdU prior to collection and stained for cell cycle analysis according to manufacturer's instructions for the BrdU Flow Kit (BD Pharmingen). p values were determined using Student's T-tests.

Senescence-associated ß-galactosidase staining. SA-ß-gal staining was performed as previously described (Dimri et al. 1995; Itahana et al. 2007) except the citric acid/sodium phosphate buffer was used at pH 5.5 and staining was performed overnight. The percent of SA-ß-gal$^+$ cells was determined by counting the number of SA-ß-gal$^+$ cells in at least 500 cells. p values were determined using Student's T-tests.

Nfib and L-myc overexpression. Nfib and L-myc were stably expressed in mouse cell lines using MSCV-Nfib-PGK-Neo and MSCV-L-myc-PGK-Puro, and selected with G418 (Invitrogen) or Puromycin (Sigma), respectively. Mouse embryonic fibroblasts (MEFs) were infected with the overexpression vectors, but did not undergo selection. The mouse Nfib cDNA was FLAG tagged, and a Kozak sequence was added before the ATG in both the L-myc and Nfib expression vectors.

Primers:

Mouse *Nfib* cDNA F: 5' CTAGAGTTAACATGATGGATTACAAAGACGATGACGATAAA

TATTCTCCCATCTGTCTC,

Mouse *Nfib* cDNA R: 5' TGACAAGATCTTCAGTTGCTTGTCTCCGCTT,

Mouse *L-myc* cDNA F: 5' ATGATCTCGAGCCACCATGGACTTCGACTCGTAT,

Mouse *L-myc* cDNA R: 5' TAGCACGGAATTCTTAGTAGCCACTGAGGTACGCGA

Mouse SCLC cell line functional experiments. Following stable expression of Nfib, L-myc or both L-myc & Nfib, cells were used in two assays. For soft agar colony formation assays, $1.5x10^4$ cells were plated in 3 cm plates in 0.4% agarose on top of a layer of 0.8% agarose (Seaplaque). Soft agar colony formation assays were done in triplicate and performed at least twice. Cultures were fed weekly and after two weeks, colonies were stained with 0.2% crystal violet and the number of colonies in at least 9 camera views per plate using a 10X objective was quantified. p values were determined using Student's T-tests. Growth curve assays were performed in triplicate and performed twice. 10^5 cells were plated in triplicate wells in 6 well plates and the number of cells was counted each day for 4 days (Coulter Counter, Beckman). Graphs represent the mean number of cells +/- standard error of the mean (SEM) of the two experiments.

MEF Transformation assays. The mouse embryonic fibroblast (MEF) experiments were performed using wild type and $p53^{-/-}$ MEFs each from two different embryos, in triplicate, and before passage 6. Following infection with L-myc and/or Nfib expression vectors, cells were used in three different assays. The low-density plating experiments were performed essentially as previously described (Sage et al. 2000), except colonies were

allowed to grow for three weeks and colonies were stained with 0.5% crystal violet in 25% methanol. In the foci formation assay, $3.8x10^5$ MEFs were plated in 6 cm plates and were performed as previously described (Sage et al. 2000) except the foci were stained using 0.5% crystal violet in 25% methanol after two weeks. All MEFs were grown in DME, 10% FBS, 1% L-glutamine and 50 units/mL Penicillin, 50 μg/mL Streptomycin, 1 mM sodium pyruvate (Sigma), non-essential amino acids (Sigma), 0.1 mM ß-mercaptoethanol (Sigma). For soft agar colony formation assays, $1.5x10^4$ cells were plated in 3 cm plates in 0.4% agarose on top of a layer of 0.8% agarose (Seaplaque). Cultures were fed weekly and after two weeks, colonies were stained with 0.2% crystal violet and the number of colonies in at least 9 camera views per plate using a 10X objective was quantified. p values were determined using Student's T-tests.

Gene expression analysis.

Microarray analysis. RNA was isolated with TRIzol (Invitrogen), labeled and hybridized to Affymetrix 430A_v2 chips according to manufacturer's instructions. Affymetrix data analysis was done using statistical tools provided by the r/Bioconductor projects (http://cran.r-project.org/; http://www.bioconductor.org/). Data import and quality control assessment was done using the packages Affy and AffyPLM and data was summarized and normalized using gcRMA (Bolstad et al. 2005a; Bolstad et al. 2005b). Differential expression analysis was carried out using limma (Smyth 2005). Prior to differential expression testing, the biological replicates of the different treatments of the 3583T3 and 3151T4 cell lines were averaged and the mean values from these replicates were

used in limma and GSEA analysis (see below). Gene expression data was deposited in Gene Expression Omnibus (GSE29533).

Gene Set Enrichment Analysis (GSEA). GSEA (http://www.broad.mit.edu/gsea/) was used to examine the distribution of groups of manually curated gene sets (http://www.broadinstitute.org/gsea/msigdb/genesets.jsp?collection=C2) within genes rank-ordered based on differential expression between the treatment classes. All the files required for these analyses and the results are available here (http://luria.mit.edu/caw_web/Dooley_Supplemental/MsigDB_v3/).

Supplemental References

Bolstad BM, Collin F, Brettschneider J, Simpson L, Cope L, Irizarry RA, and Speed TP. 2005a. Quality assessment of affymetrix genechip data. in Bioinformatics and Computational Biology Solutions using R and Bioconductor (eds. R. Gentleman, V. Carey, S. Dudoit, R. Irizarry, and W. Huber), pp. 33-47. Springer, New York.

Bolstad BM, Irizarry RA, Gautier L, and Wu Z. 2005b. Preprocessing high-density oligonucleotide arrays. in Bioinformatics and Computational Biology Solutions using R and Bioconductor (eds. R. Gentleman, V. Carey, S. Dudoit, R. Irizarry, and W. Huber), pp. 13-32. Springer, New York.

Chung Y-J, Jonkers J, Kitson H, Fiegler H, Humphray S, Scott C, Hunt S, Yu Y, Nishijima I, Velds A et al. 2004. A Whole-Genome Mouse BAC Microarray With 1-Mb Resolution for Analysis of DNA Copy Number Changes by Array Comparative Genomic Hybridization. Genome Research 14: 188-196.

Dimri GP, Lee X, Basile G, Acosta M, Scott G, Roskelley C, Medrano EE, Linskens M, Rubelj I, and Pereira-Smith O. 1995. A biomarker that identifies senescent human cells in culture and in aging skin in vivo. Proc Natl Acad Sci 92: 9363-9367.

Itahana K, Campisi J, and Dimri GP. 2007. Methods to detect biomarkers of cellular senescence: the senescence-associated beta-galactosidase assay. Methods Mol Biol 371: 21-31.

Meylan E, Dooley AL, Feldser DM, Shen L, Turk E, Ouyang C, and Jacks T. 2009. Requirement for NF-κB signalling in a mouse model of lung adenocarcinoma. Nature 462: 104-107.

Sage J, Mulligan GJ, Attardi LD, Miller A, Chen S, Williams B, Theodorou E, and Jacks T. 2000. Targeted disruption of the three Rb-related genes leads to loss of G1 control and immortalization. Genes & Development 14: 3037-3050.

Smyth GK. 2005. Limma: Linear Models for microarray data. in Bioinformatics and Computational Biology Solutions using R and Bioconductor (eds. R. Gentleman, V. Carey, S. Dudoit, R. Irizarry, and W. Huber), pp. 397-420. Springer, New York.

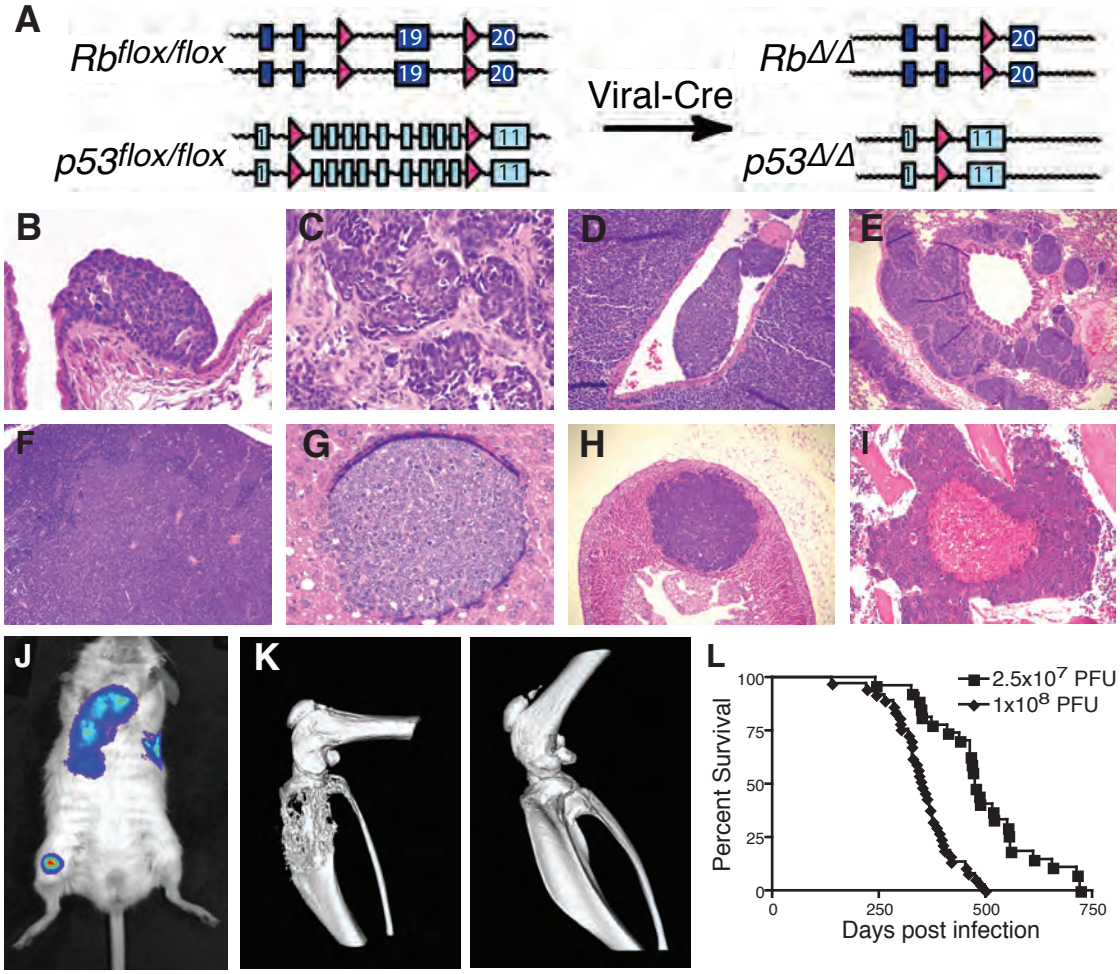
A
Rb flox/flox
19
20
19
20
p53 flox/flox
11
11
Viral-Cre
Rb Δ/Δ
20
20
p53 Δ/Δ
11
11
B
C
D
E
F
G
H
I
J
K
L
2.5x10^7 PFU
1x10^8 PFU
Percent Survival
100
75
50
25
0
0
250
500
750
Days post infection

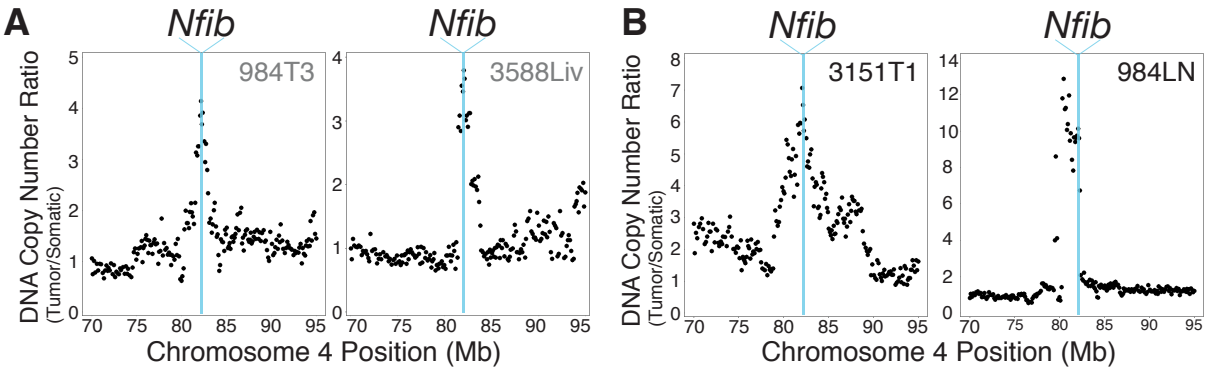
A
Nfib
Nfib
984T3
3588Liv
DNA Copy Number Ratio
(Tumor/Somatic)
Chromosome 4 Position (Mb)
B
Nfib
Nfib
3151T1
984LN
DNA Copy Number Ratio
(Tumor/Somatic)
Chromosome 4 Position (Mb)

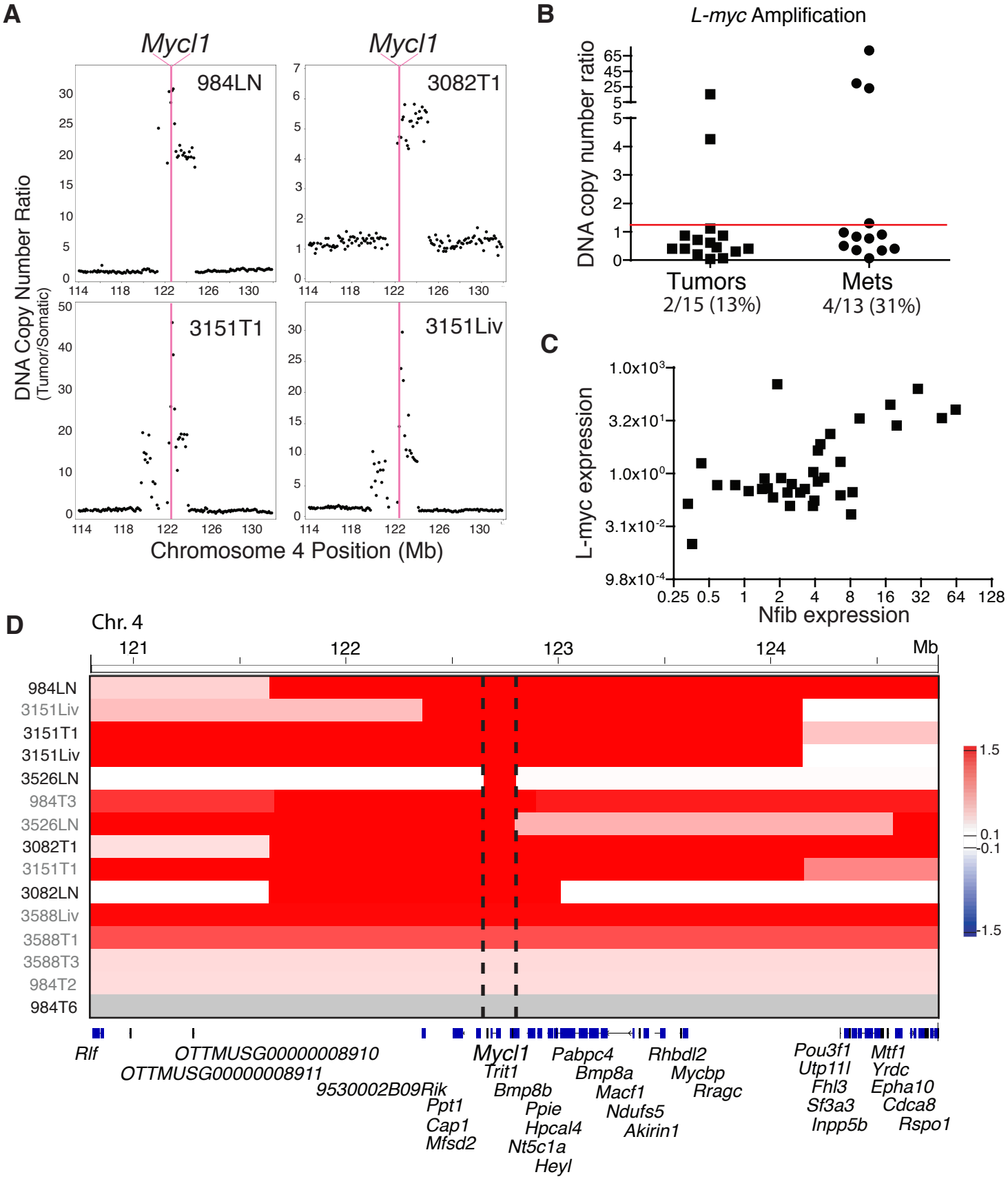
A
Mycl1
Mycl1
984LN
3082T1
3151T1
3151Liv
DNA Copy Number Ratio
(Tumor/Somatic)
Chromosome 4 Position (Mb)
B
L-myc Amplification
DNA copy number ratio
Tumors
2/15 (13%)
Mets
4/13 (31%)
C
L-myc expression
Nfib expression
D
Chr. 4
121
122
123
124
Mb
984LN
3151Liv
3151T1
3151Liv
3526LN
984T3
3526LN
3082T1
3151T1
3082LN
3588Liv
3588T1
3588T3
984T2
984T6
Rlf
OTTMUSG00000008910
OTTMUSG00000008911
9530002B09Rik
Ppt1
Cap1
Mfsd2
Mycl1
Trit1
Bmp8b
Ppie
Hpcal4
Nt5c1a
Heyl
Pabpc4
Bmp8a
Macf1
Ndufs5
Akirin1
Rhbdl2
Mycbp
Rragc
Pou3f1
Utp11l
Fhl3
Sf3a3
Inpp5b
Mtf1
Yrdc
Epha10
Cdca8
Rspo1

A

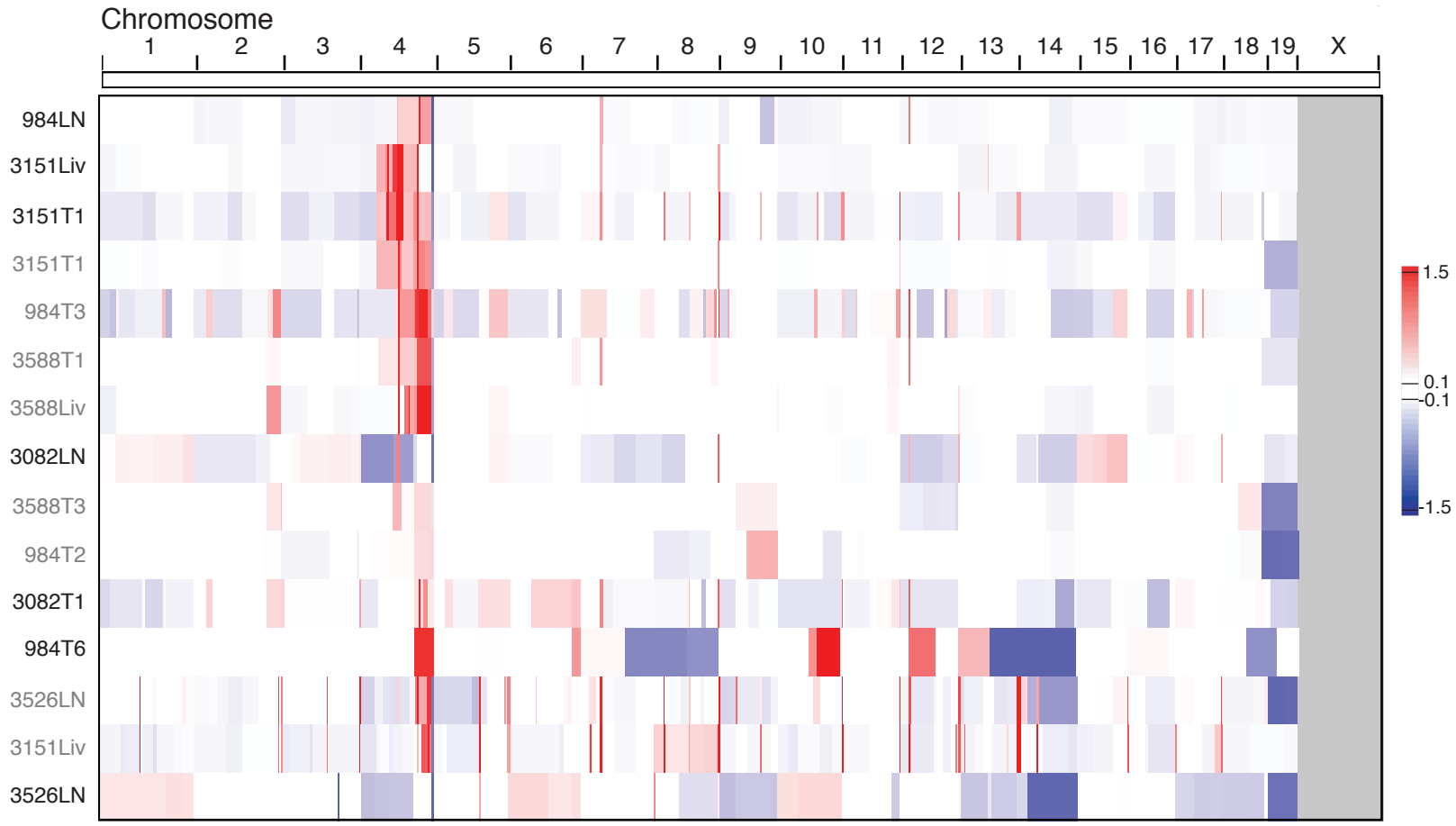
Chromosome
1
2
3
4
5
6
7
8
9
10
11
12
13
14
15
16
17
18
19
X
984LN
3151Liv
3151T1
3151T1
984T3
3588T1
3588Liv
3082LN
3588T3
984T2
3082T1
984T6
3526LN
3151Liv
3526LN
1.5
0.1
-0.1
-1.5

A

L-myc \ *Nfib*	amplified	not amplified
amplified	4	2
not amplified	12	10

B

L-MYC \ *NFIB*	amplified	not amplified
amplified	11	12
not amplified	5	18

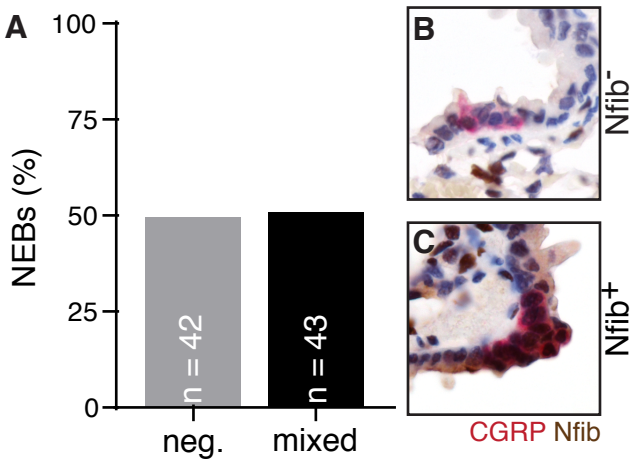
A
100
75
50
25
0
NEBs (%)
n = 42
n = 43
neg.
mixed
B
Nfib-
C
Nfib+
CGRP Nfib

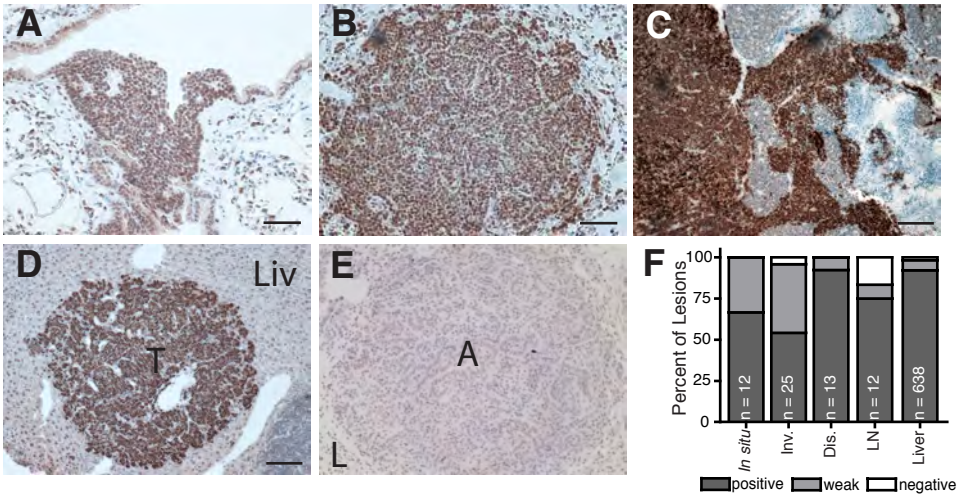
A
B
C
D
Liv
T
E
A
L
F
Percent of Lesions
100
75
50
25
0
In situ n = 12
Inv. n = 25
Dis. n = 13
LN n = 12
Liver n = 638
positive
weak
negative

A

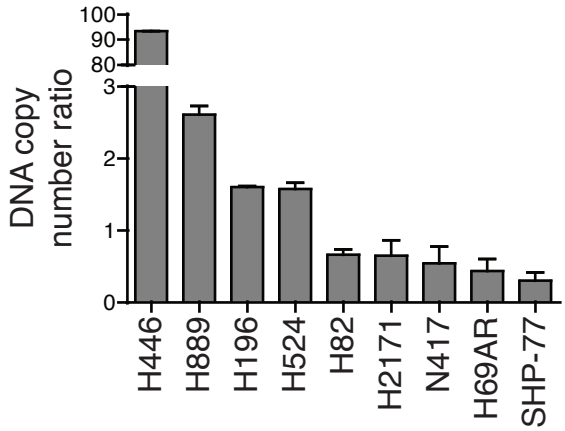
DNA copy number ratio
100
90
80
3
2
1
0
H446
H889
H196
H524
H82
H2171
N417
H69AR
SHP-77

A

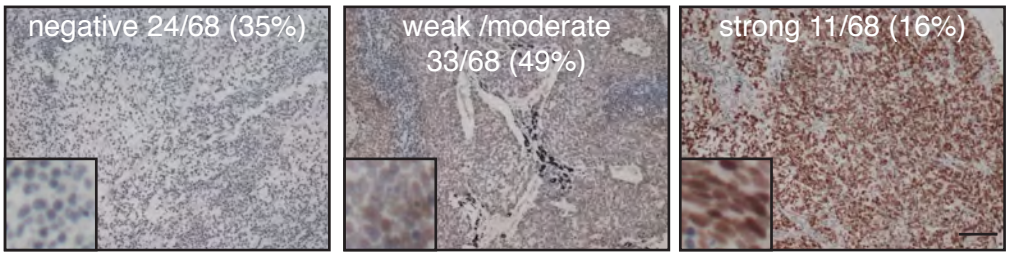

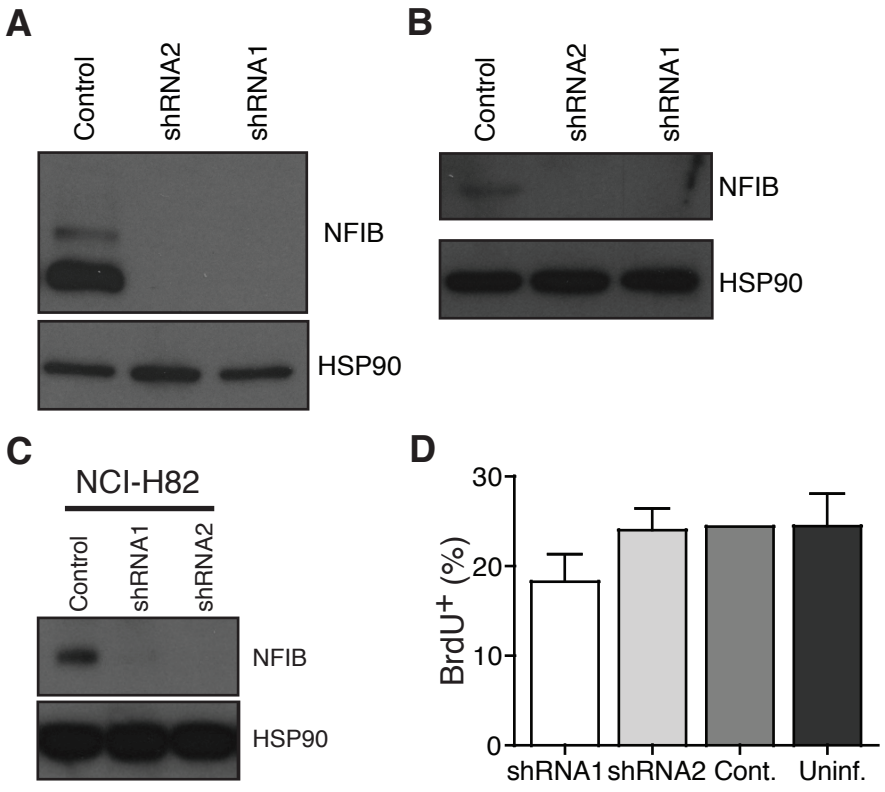
A
Control
shRNA2
shRNA1
NFIB
HSP90
B
Control
shRNA2
shRNA1
NFIB
HSP90
C
NCI-H82
Control
shRNA1
shRNA2
NFIB
HSP90
D
BrdU+ (%)
30
20
10
0
shRNA1
shRNA2
Cont.
Uninf.

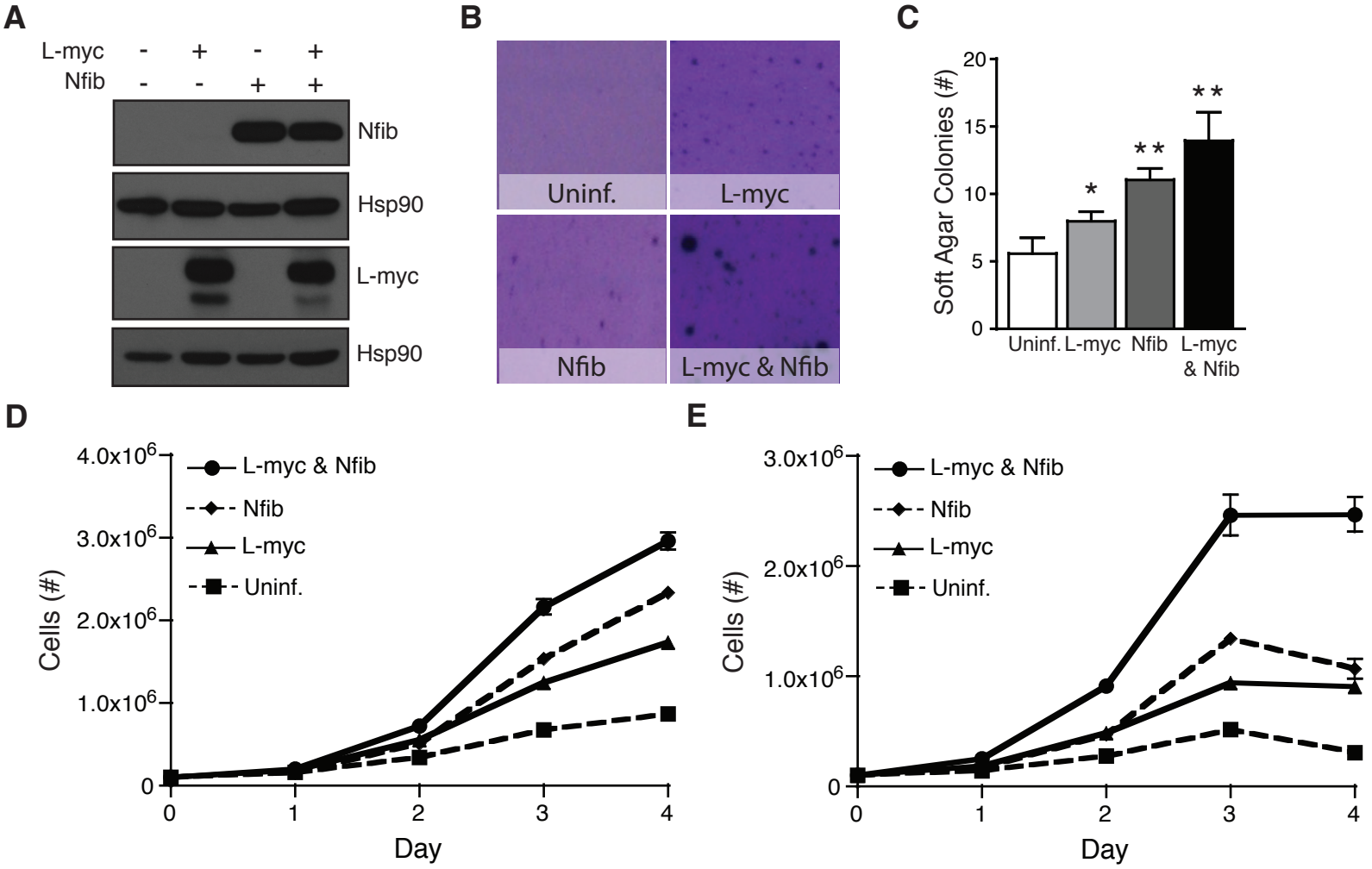
A
L-myc - + - +
Nfib - - + +
Nfib
Hsp90
L-myc
Hsp90
B
Uninf.
L-myc
Nfib
L-myc & Nfib
C
Soft Agar Colonies (#)
20
15
10
5
0
*
**
**
Uninf.
L-myc
Nfib
L-myc & Nfib
D
Cells (#)
4.0x10^6
3.0x10^6
2.0x10^6
1.0x10^6
0
L-myc & Nfib
Nfib
L-myc
Uninf.
0
1
2
3
4
Day
E
Cells (#)
3.0x10^6
2.0x10^6
1.0x10^6
0
L-myc & Nfib
Nfib
L-myc
Uninf.
0
1
2
3
4
Day

Curated Gene Sets	NES	Gene Set Description
Korkola_Teratoma	2.13	Genes predicting the teratoma subtype of nonseminomatous male germ cell tumors
Browne_Interferon_Responsive_Genes	2.13	Genes up-regulated in primary fibroblasts following treatment with interferon alpha for 6 hours
Lastowska_Coamplified_with_MYCN	1.92	Genes co-amplified with MYCN in primary neuroblastoma tumors
Lian_LIPA_Targets_6M	-2.65	Genes up-regulated in lungs from 6 month old LIPA knockout mice
Markey_RB1_Chronic_LOF_Dn	-2.53	Genes down-regulated in MEFs isolated from RB1 knockout mice
Yu_MYC_Targets_Dn	-1.95	Genes down-regulated in B cell lymphomas expressing an activated form of MYC

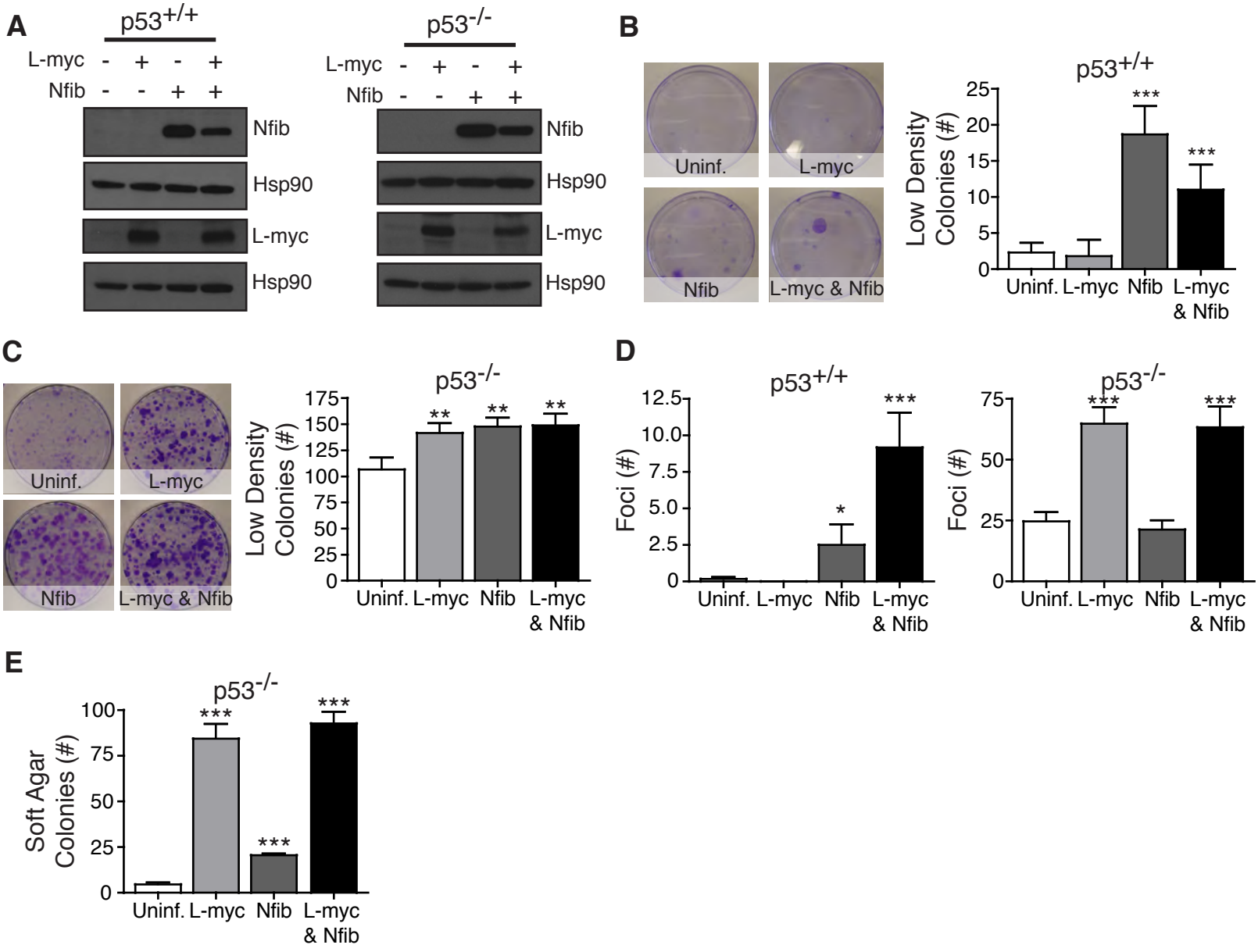
A
p53+/+
L-myc - + - +
Nfib - - + +
Nfib
Hsp90
L-myc
Hsp90
p53-/-
L-myc - + - +
Nfib - - + +
Nfib
Hsp90
L-myc
Hsp90
B
Uninf.
L-myc
Nfib
L-myc & Nfib
p53+/+
Low Density Colonies (#)
25
20
15
10
5
0
***
***
Uninf. L-myc Nfib L-myc & Nfib
C
Uninf.
L-myc
Nfib
L-myc & Nfib
p53-/-
Low Density Colonies (#)
175
150
125
100
75
50
25
0
**
**
**
Uninf. L-myc Nfib L-myc & Nfib
D
p53+/+
Foci (#)
12.5
10.0
7.5
5.0
2.5
0
*
***
Uninf. L-myc Nfib L-myc & Nfib
p53-/-
Foci (#)
75
50
25
0
***
***
Uninf. L-myc Nfib L-myc & Nfib
E
p53-/-
Soft Agar Colonies (#)
100
75
50
25
0
***
***
***
Uninf. L-myc Nfib L-myc & Nfib

Sample	DNA Source	Total reads	Confidently aligned reads
Somatic1	tail	4064293	1694532
Somatic2	tail	5212109	2858180
129Som	tail	5430824	3470755
Total Somatic		14707226	8023467
984LN	cell line	4514631	3065735
984LN	fresh tissue	5909969	3096862
984T6	cell line	5910893	3938360
984T2	fresh tissue	5946141	3880381
984T3	fresh tissue	6336110	3534753
3588T1	fresh tissue	6715350	4414906
3588T3	fresh tissue	6590516	4391195
3588Liv	fresh tissue	6359123	4262816
3082T1	cell line	6101749	4261614
3082LN	cell line	6312999	4357165
3151T1	fresh tissue	6505090	4081703
3151Liv	cell line	6874539	4666647
3526LN	cell line	6955500	3993508
3151T1	cell line	6066834	1649405
3151Liv	fresh tissue	8522947	5861214
3526LN	fresh tissue	7552605	4940323